Magnetic Reconnection and Current-Sheet Formation at X-Type Neutral Points

R. S. Steinolfson

Department of Space Sciences, Southwest Research Institute, San Antonio, Texas

L. Ofman[1] and P. J. Morrison

Institute for Fusion Studies, University of Texas, Austin, Texas

Numerical solutions of the nonlinear, resistive magnetohydrodynamic (MHD) equations are used to study the evolution of a perturbed or stressed x-type neutral point. By performing individual simulations for both compressible and incompressible plasmas, we are able to demonstrate that the important physics for this problem involves just the interaction between the plasma flow velocity and the magnetic field and that the thermodynamics has a relatively passive effect. We have also done separate simulations for both solid, conducting wall boundary conditions at a fixed distance from the x-point and for open boundary conditions that adjust as required by the evolving solution within the boundaries. With solid, conducting wall boundary conditions, our solutions for azimuthally symmetric disturbances agree (for essentially linear perturbations) with those obtained in previous analytic linear studies. In this case the stressed x-point relaxes back to the unstressed state on a time scale somewhat shorter than the time scale for the linear resistive tearing mode. Perturbations that are not azimuthally symmetric can relax even faster than the symmetric modes. When the conditions at the boundary are free to adjust, the disturbances grow in amplitude on an Alfvén time scale with the eventual formation of a current sheet separating two y-points. This rapid growing behavior is, of course, in sharp contrast to the relatively slow decaying solutions obtained with closed boundaries. The growing solutions qualitatively agree with previous analytic x-point solutions that have been suggested as an explanation for the rapid energy conversion in flares and substorms.

1. INTRODUCTION

Localized regions within a plasma with an imbedded magnetic field containing points or lines at which the magnetic field strength vanishes have long been recognized as having important and unique topographical features. In a plasma for which the physical variables do not change in one dimension (the ignorable coordinate), one such region is the x-type neutral point (also referred to here as an x-point or neutral point), which becomes a neutral line along the ignorable coordinate. The x-point is of particular interest in solar physics since this may be the location of the rapid conversion of magnetic energy to other forms of energy in solar flares, as suggested by *Giovanelli* [1947]. *Dungey* [1953] quantified the suggestion by Giovanelli and showed that x-type neutral points were unstable and that a small perturbation initiated a rapid increase in the current at the neutral point. *Chapman and Kendall* [1963] used a more complete quantitative analysis than Dungey and were able to show that the instability grew on a time scale comparable to an Alfvén crossing time. In addition, for the Chapman and Kendall solution the x-point eventually changed to a current sheet with y-points at the ends. *Syrovatsky* [1966] later included this instability mechanism and the current sheet formation in a solar flare model. As the above references indicate, much of the early interest in perturbed x-type neutral points concentrated on the growing solutions and the potential application to explosive phenomena such as flares and auroral discharges [*Akasofu and Chapman*, 1961].

More recently, there has been some effort to examine solutions for perturbed x-type neutral points that do not grow

[1]Currently at NASA Goddard Space Flight Center, Greenbelt, MD

Space Plasmas: Coupling Between Small and Medium Scale Processes
Geophysical Monograph 86

in time but rather decay back to the unperturbed configuration [*Craig and McClymont*, 1991; *Hassam*, 1991; *Craig and Watson*, 1992]. A primary interest in these studies has been to demonstrate that reconnection at the neutral point occurs at a rate faster than either the classical reconnection rate for the tearing instability [*Furth, Killeen, and Rosenbluth*, 1973] or the slightly faster rate predicted by *Sweet* [1958] and *Parker* [1963]. An important difference between these decaying solutions and the above growing solutions is the form of the outer boundary conditions at some fixed distance from the x-point. The perturbed magnetic flux must vanish at a solid, conducting wall surrounding the neutral point for the decaying solutions, while it must be allowed to adjust as required by conditions within the boundary for the growing solutions. In addition, for the two-dimensional cylindrical geometry often used in studies of the decaying solutions, the perturbed magnetic flux must depend only on radial distance from the neutral point in order to obtain the fast reconnection.

In the present study we numerically solve the two-dimensional, nonlinear, dissipative magnetohydrodynamic (MHD) equations for both a compressible and an incompressible plasma. We consider both the solid, conducting wall boundary conditions used in previous decaying solution studies as well as open or free boundary conditions for the growing solutions. We begin with solid, conducting wall boundary conditions, which should be applicable to fusion devices and laboratory plasmas, and simulate the relaxation of a perturbed or stressed x-point back to the initial potential state and show that our results are in quantitative agreement with those from earlier studies. When the boundaries are allowed to be open, which should have application to more general space plasmas and to flares and auroral discharges, the perturbation grows at a rate comparable to a relevant Alfvén time scale and the x-point evolves into a current sheet as predicted in the more approximate studies indicated above.

Our objectives are twofold. First of all, by applying both incompressible and compressible theory to the same problem, we are able to demonstrate, for this application, that the important physics lies not in the plasma thermodynamic properties but rather in the coupling between the inertial and magnetic (including resistivity effects) terms. Secondly, by using the same numerical codes with different outer boundary conditions, we show the dramatic influence the boundary conditions can have on the computed solutions; i.e., decaying solutions with solid, conducting walls and growing solutions when the plasma motion and magnetic field are not restricted at the outer boundary.

2. MHD EQUATIONS AND NUMERICAL SOLUTION

We make the usual assumption that MHD adequately describes the essential physics in this problem. By further assuming that the plasma resistivity is constant and isotropic and that gravitational and viscous effects are negligible, the compressible equations can be written in nondimensional form as follows:

$$\frac{\partial \rho}{\partial t} + \nabla \cdot (\rho \boldsymbol{u}) = 0 , \tag{1a}$$

$$\rho \frac{d\boldsymbol{u}}{dt} = -\frac{\beta}{2}\nabla p + (\nabla \times \boldsymbol{B}) \times \boldsymbol{B} , \tag{1b}$$

$$\frac{\partial \boldsymbol{B}}{\partial t} = \nabla \times (\boldsymbol{u} \times \boldsymbol{B}) - \frac{1}{S}\nabla \times (\nabla \times \boldsymbol{B}) , \tag{1c}$$

$$\frac{d}{dt}\left(\frac{p}{\rho^{\gamma}}\right) = 0 , \tag{1d}$$

where d/dt indicates the convective derivative. The physical quantities are the density ρ, the velocity $\boldsymbol{u}$, the magnetic field $\boldsymbol{B}$, and the thermal pressure p. The specific heat ratio is represented by γ, which is taken here to be 5/3. The equations have been put in dimensionless form by normalizing time to a relevant Alfvén time $\tau_a = a(4\pi\rho_o)^{1/2}/B_o$, distance to the quantity a, which is a representative scale length for changes in the magnetic field, velocity to a/τ_a, thermodynamic quantities to their initial, uniform values (ρ_o and p_o), and magnetic field strength to the average value over the outer boundary B_o. The two parameters are the plasma beta ($\beta = 8\pi p_o/B_o^2$, the ratio of thermal pressure to magnetic pressure) and the Lundquist number ($S = \tau_r/\tau_a$, the ratio of the resistive diffusion time to the Alfvén time). The resistive diffusion time is defined as $\tau_r = 4\pi a^2/c^2\eta$, where c is the light speed and η is the plasma resistivity. We further make the assumption that the initial equilibrium magnetic field is externally maintained so it is not resistively dissipated.

The two-dimensional (2-D) incompressible MHD equations are obtained by writing the magnetic field in terms of a stream function using $\boldsymbol{B} = \nabla\psi \times \boldsymbol{e}_z$ and the velocity in terms of a flux function $\boldsymbol{u} = \nabla\phi \times \boldsymbol{e}_z$, where $\boldsymbol{e}_z$ is the unit vector in the ignorable direction z in a Cartesian coordinate system. By then taking the curl of the momentum equation

(1b) to eliminate the thermal pressure p and setting the constant density to unity, the equations can be written as:

$$\frac{\partial \psi}{\partial t} = -\frac{\partial \phi}{\partial y}\left(\frac{\partial \psi}{\partial x}+x\right) + \frac{\partial \phi}{\partial x}\left(\frac{\partial \psi}{\partial y}-y\right) - \frac{1}{S}J , \quad (2a)$$

$$\frac{\partial \omega}{\partial t} = -\frac{\partial \phi}{\partial y}\frac{\partial \omega}{\partial x} + \frac{\partial \phi}{\partial x}\frac{\partial \omega}{\partial y} + \left(\frac{\partial \psi}{\partial y}-y\right)\frac{\partial J}{\partial x} - \left(\frac{\partial \psi}{\partial x}+x\right)\frac{\partial J}{\partial y} , \quad (2b)$$

where $J = -\nabla\psi_\perp{}^2$ is the z-component of the current density, $\omega = -\nabla\phi_\perp{}^2$ is the z-component of the vorticity, and $\nabla_\perp{}^2 = \partial^2/\partial x^2 + \partial^2/\partial y^2$ with $\partial/\partial z = 0$. Note that the dimensionless parameter β does not enter into the incompressible equations. The thermodynamics uncouples from the evolution of the plasma velocity and the magnetic field with this approximation.

The compressible equations are solved numerically using an explicit finite differencing scheme of the Lax-Wendroff type [*Rubin and Burstein*, 1967] with a smoothing term suggested by *Lapidus* [1967]. The equations are solved in the r,θ plane of a cylindrical coordinate system with a computational domain limited by $0 \le r \le r_m$, $0 \le \theta \le \pi/2$. All physical quantities are either symmetric or antisymmetric at the $\theta = 0$ and $\theta = \pi/2$ boundaries. The outer boundary conditions at $r = r_m$ will be discussed separately for each of the two studies in the following sections. The incompressible equations are solved numerically using an alternating-direction implicit method as discussed further by *Steinolfson and van Hoven* [1984]. These equations are solved in the x,y plane of a Cartesian geometry with a computational domain limited by $-x_m \le x \le x_m$, $-y_m \le y \le y_m$. As for the compressible case, the outer boundary conditions will be discussed in the following sections.

The equilibrium potential magnetic field for the compressible study is $B_o = r(\sin 2\theta e_r + \cos 2\theta e_\theta)$. The initial equilibrium magnetic flux for the incompressible study can be written as $\psi_o = x^2 - y^2$, in which case the equilibrium potential magnetic field components are $B_{xo} = -2y$ and $B_{yo} = -2x$. The initial magnetic field for both cases contains an x-point, as shown for Cartesian geometry in Figure 1. The perturbation magnetic fields used in the separate studies will be discussed later.

3. DECAYING SOLUTIONS: RECONNECTION AT THE X-POINT

Hassam [1991] and *Craig and McClymont* [1991] investigated the behavior of perturbed x-points using linearized, compressible MHD with the low-beta approximation so thermal pressure gradients could be neglected. More importantly, in terms of the types of solutions they obtained, they assumed that the plasma was confined within solid, conducting walls. They solved the equations in the r,θ plane of a cylindrical coordinate system and showed that they can be reduced to a single, second-order partial differential equation for the perturbed magnetic flux function. Separation of variables, with an assumed time and angular dependence given by $\exp(\lambda t + im\theta)$, is used to reduce the equation to an ordinary differential equation in r. It is then argued that only the $m = 0$ (azimuthally symmetric) modes involve reconnection at the x-point, and therefore, the analysis is limited to the $m = 0$ modes. For these modes the approximate expressions for the oscillation and decay times of the fundamental radial mode ($n = 0$, the radial mode with longest wavelength) are derived as:

$$\tau_{osc} \approx 2 \ln S , \qquad \tau_{dec} \approx 2(\ln S)^2/\pi^2 . \quad (3)$$

Ofman [1992] has taken the above analysis one step further and has derived the general linear solution valid for any radial and azimuthal mode. His solution for the $m = n = 0$ mode is given by the solid curve in Figure 2, and the above approximate solution is given by the dashed line. As a check on the nonlinear incompressible code, the decay rate

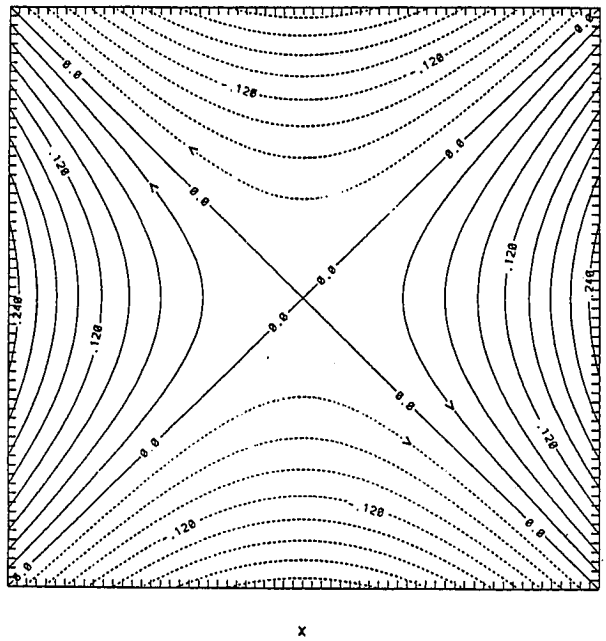

Fig. 1. The equilibrium magnetic field configuration containing an x-point. These are contour lines of the magnetic flux function ψ_o defined in the text.

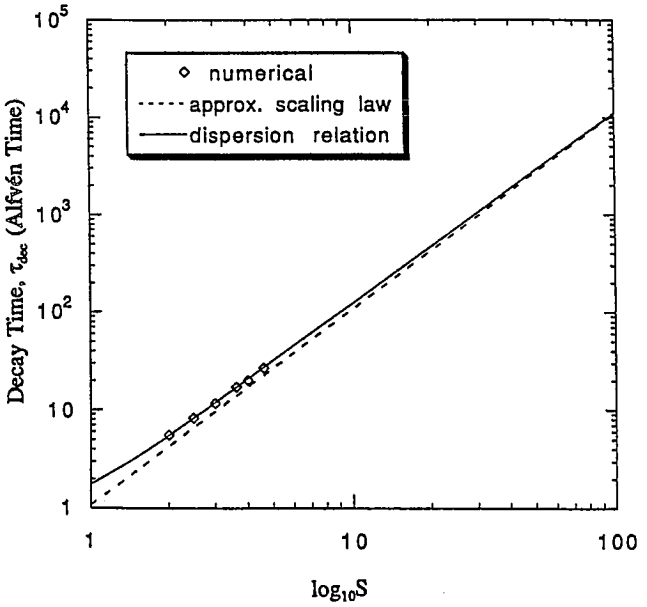

Fig. 2. The dependence of the decay time on S for the $m = n = 0$ mode. The dispersion relation is from *Ofman* [1992], the dashed curve is for τ_{dec} in equation (3), and the boxes indicate results from the numerical computation.

for small perturbations was computed for $10^2 \le S \le 4 \times 10^4$, and the results are compared with the analytic solutions in the figure. The perturbed magnetic flux function for this simulation is given by:

$$\psi_1 = A_i\,(x_m^2 - x^2)\,(y_m^2 - y^2)\,\exp(-5(x^2+y^2)) \qquad (4)$$

with $A_i = 10^{-2}$. The initial perturbation was selected to have approximate azimuthal symmetry ($m = 0$) near the origin, to vanish at the edges of the box ($x_m = y_m = 1$), and to decrease monotonically with distance from the origin ($n = 0$). Since the computational box is square, the disturbance will always have some azimuthal dependence at least near the edges of the box. Both the magnetic flux function ψ and the stream function ϕ are required to remain zero at the outer boundaries.

The relaxation of the perturbed x-point for the $S = 10^4$ case in Figure 2 is shown in Figures 3-5. The temporal decay and oscillation of the perturbed magnetic energy in the x-component of the field (curve A), the perturbed magnetic energy in the y-component of the field (curve B) and the total (magnetic plus kinetic, curve C) energies are given in Figure 3. These energies are computed by integrating over the entire region. The variation of the magnetic flux at the origin [$\psi(0,0,t)$] is shown in Figure 4. As discussed earlier, the magnetic field reconnects whenever $\psi(0,0,t)\neq 0$. This reconnection of the field when $\psi(0,0,t)\neq 0$ can be seen from plots of the magnetic field lines at three times during the oscillating decay in Figure 5. The results in Figure 5(a) are at the first minimum of $\psi(0,0,t)$ at $t \approx 7$, those in Figure 5(b) are at the second zero of $\psi(0,0,t)$ at $t \approx 12$, and those in

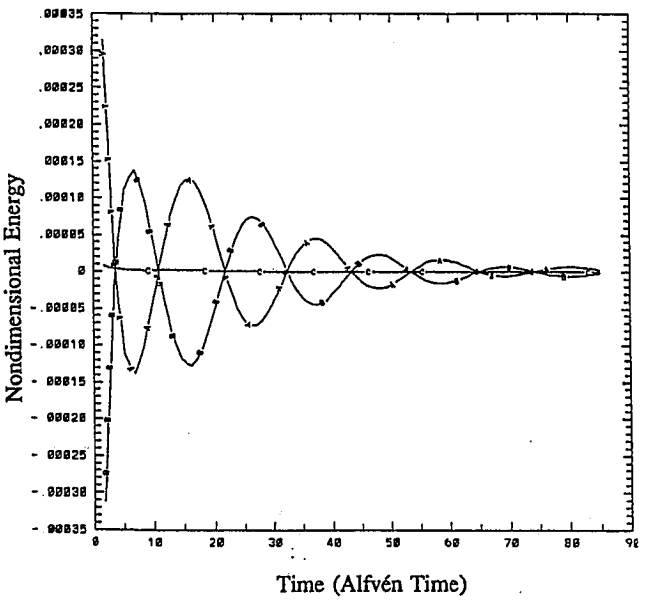

Fig. 3. The relaxation of the perturbed energies integrated over the numerical box for a disturbed x-point. The curves represent the x- and y-components of the magnetic energy (curves A and B) and the total energy (curve C).

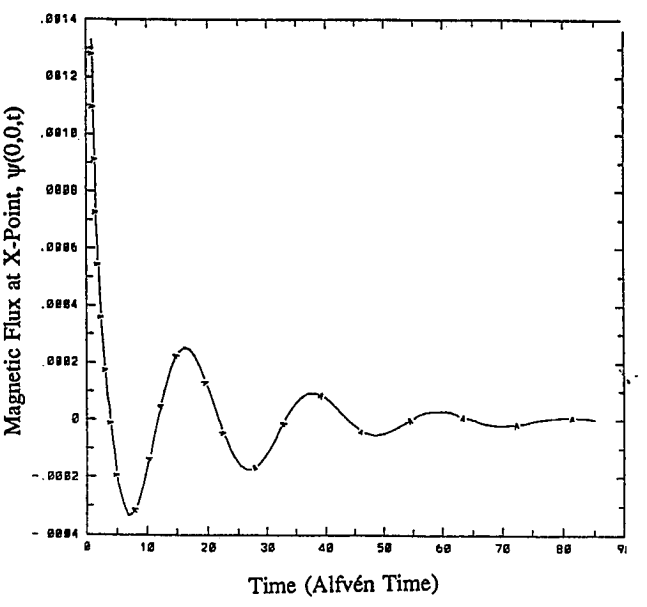

Fig. 4. The temporal variation of the magnetic flux at the x-point [$\psi(0,0,t)$].

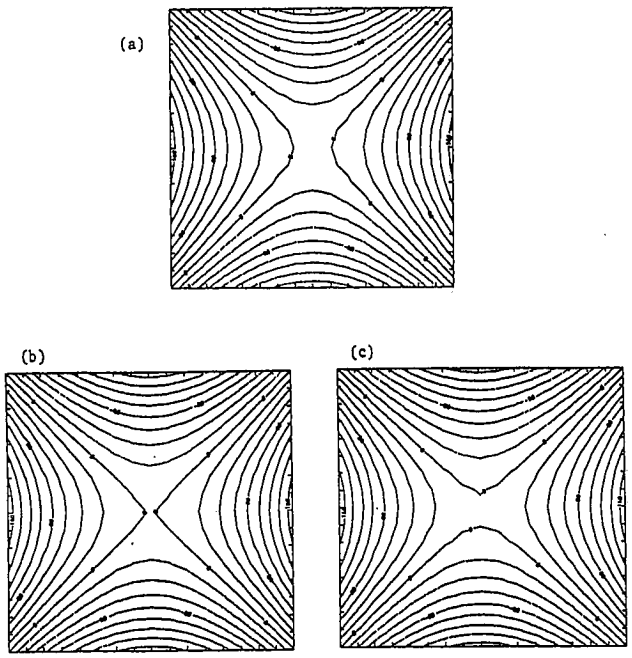

Fig. 5. Magnetic field lines at various times during the oscillating decay. The field lines in (a) are at the first minimum in $\psi(0,0,t)$ in Figure 4, those in (b) are at the second zero in $\psi(0,0,t)$, and those in (c) are at the time of the following maximum in $\psi(0,0,t)$.

Figure 5(c) are at the following maximum of $\psi(0,0,t)$ at $t \approx 16$. The reconnection oscillates between the field lines to the left and right of the x-point (at the center of the figure) and the field lines above and below the x-point. In Figure 5(b) the magnetic flux function vanishes at the origin, there is very little reconnection, and the magnetic configuration is nearly force-free. The oscillations are damped by the resistive reconnection, and the final state is the force-free x-point configuration given by ψ_o.

The decay and oscillation times computed with the compressible code also agree with the analytic results given above. The $m = 0$ perturbation (defined in terms of the magnetic flux function) used in this case is $B_\theta = A_c \sin \pi r$ for $0 \le r \le 1$, and the results in Figure 6 are for $A_c = 10^{-3}$ and $S = 10^4$. The outer boundary is located at $r = 1$ where the boundary conditions are such that the thermodynamic quantities remain fixed at their initial values, the flow is parallel to the boundary, and the component of the magnetic field parallel to the boundary remains fixed. The quantity shown in the figure is the perturbed component of the magnetic field at $\theta = \pi/2$, which is calculated as $\Delta B_\theta = [B_\theta(r_i,\pi/2,t)-B_\theta(r_i,\pi/2,0)]/B_\theta(r_i,\pi/2,0)$ where $r_i = 0.02,0.04,0.06,0.08,0.10$ (curves A-E, respectively). The minor phase differences at the various radii are due to nonlinear effects and can be made arbitrarily small by reducing the magnitude

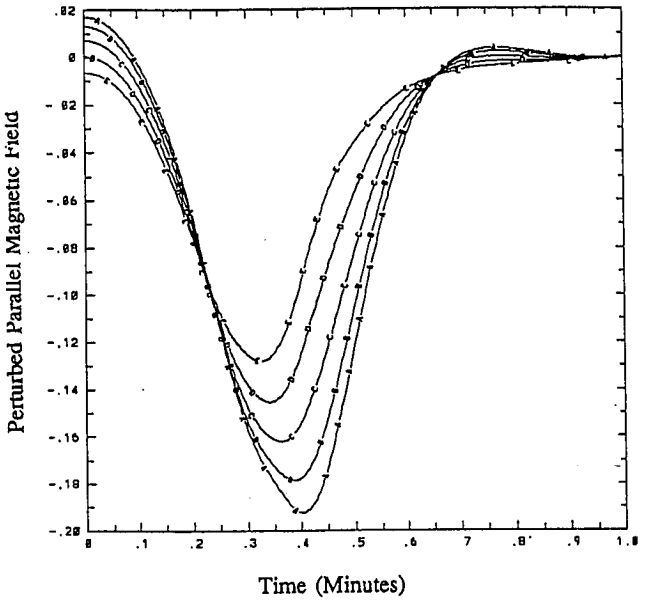

Fig. 6. The temporal decay of the perturbed component of the azimuthal magnetic field at $\theta = \pi/2$ and at several radial locations r_i near the x-point ($r_i = 0.02,0.04,0.06,0.08,0.10$).

of the initiating perturbation (reduce A_c).

4.0 GROWING SOLUTIONS: CURRENT SHEET FORMATION

The boundary conditions at the outer boundary are now changed so that this boundary is open or free, as opposed to the closed boundary considered in the previous section. Another way to view the present boundary conditions is that they are now able to adjust to changes occuring within the region of interest rather than being fixed by some external means. The boundary values are computed by setting the perturbed value of each physical quantity at the boundary equal to the respective value at the grid point next to the boundary (zero-order extrapolation).

The results shown in Figure 7 after the solution has evolved for 5.3 Alfvén times are obtained from the incompressible code using the same initial perturbation as used in the above section. The transition to the sheet current seen in the plot of the contours of ψ in Figure 7(a) occurs approximately on an Alfvén time scale. The formation of the sheet current involves large flow vortices as shown in the contour plots of the velocity potential in Figure 7(b). The flow velocity is parallel to the contours with the dashed-line contours representing clockwise rotation and the solid-line contours indicating counter-clockwise rotation.

The formation of a current sheet in the compressible simlation is seen in the results presented in Figures 8-10.

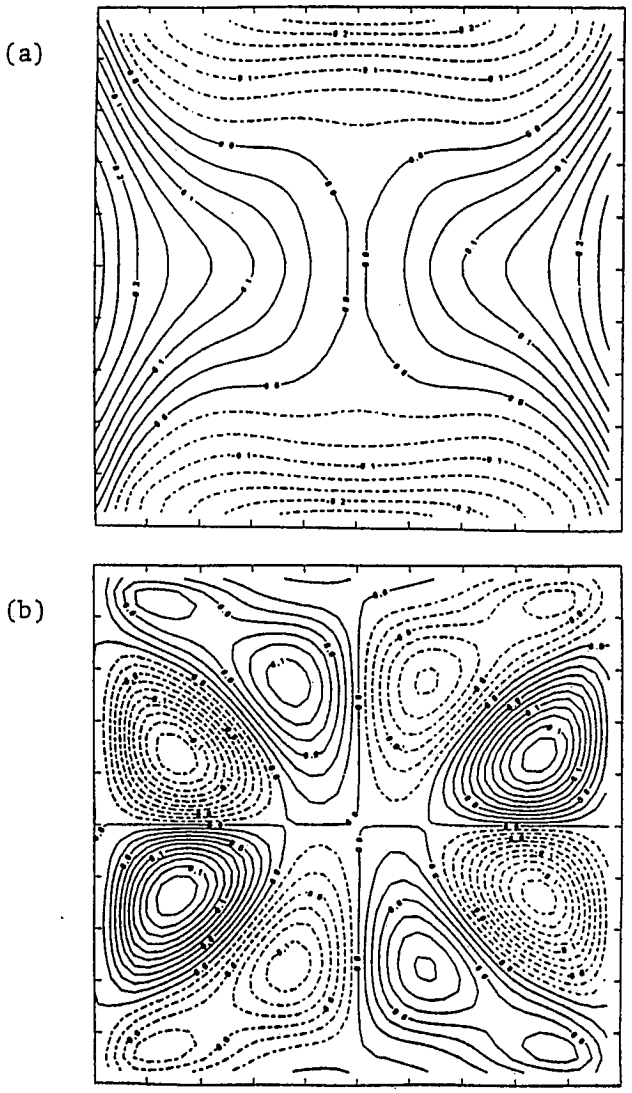

Fig. 7. The development of a sheet current in the incompressible MHD model. The magnetic field lines (contours of ψ) are shown in (a) and contours of the stream function (ϕ) are shown in (b). The flow velocity is parallel to the indicated ϕ contours with the dashed contours representing clockwise rotation and the solid contours representing counter-clockwise rotation.

The calculation extends out to $r = 2$, although the perturbation is the same as used in the previous section for the compressible solution (with $A_c = 0.05$) and only exists out to $r = 1$. The reason for extending the computation beyond the perturbation will be discussed later. The symmetries (or antisymmetries) at $\theta = \pi/2$ (the vertical axis at the center of the panels in Figures 8 and 9) were used so the solution could be shown for $0 \leq \theta \leq \pi$. The magnetic field lines and velocity vectors are shown at the same three times in Figures 8 and 9. The formation of the current sheet can be seen clearly in Figure 8(b). The center of the sheet eventually becomes a magnetic island (Figure 8(c)) separating two x-points that propagate radially away from each other. The velocity vectors have the same general pattern at all times in Figure 9 although the maximum velocity increases by almost two orders of magnitude between the times used for the top and bottom panels.

The temporal behavior of the radial components of the perturbed magnetic field and the velocity at several radial locations (r_i = 0.2,0.4,0.6,0.8,1.0,1.2,1.4,1.6,1.8,2.0 for curves A-J) along a line at $\theta = 10°$ is given in Figure 10. These curves illustrate a couple of points. First of all, the large increase in the radial field begins near the original x-point location ($r = 0$) and propagates outward. Note also that the radial component peaks and then decreases as the island forms. Also, the radial velocity increases to a larger maximum before decreasing as the x-points travel outward since the reconnection then occurs in a stronger magnetic field region, since the initial magnetic field increases with radius.

As mentioned above, the computation extends one unit in radius beyond the maximum of the initial perturbation. If the calculation did only go out to $r = 1$, the results are almost identical to those shown here with the difference that the eruptive phase begins just a little earlier. The reason the eruption then begins earlier is that, after the transients from the initial perturbation decay away, the solution (primarily the velocity) must evolve into a particular pattern throughout the entire simulation region before the eruption begins. The initial transients can be seen at early times in the temporal plots in Figure 10. The time to set up this special initial state for the eruptive behavior naturally increases as the size of the numerical box increases. It now becomes easy to understand why the growing solutions do not develop when the radial velocity is forced to be zero at the outer boundary since the necessary initial state cannot be established.

It is important to realize that these growing solutions develop from physical conditions in the vicinity of the initial x-point. They are not a result of doing something special at the outer boundaries like pushing the field lines together or imposing an electric field. All that is required at the outer boundaries is that they be open so an appropriate state (after the transients due to the initial perturbation vanish) can be established. Once the eruption begins it continues to grow explosively with the x-points traveling outward into regions of stronger magnetic fields.

5.0 SUMMARY

The evolution of perturbed x-type neutral points has been studied using numerical solutions of both compressible and

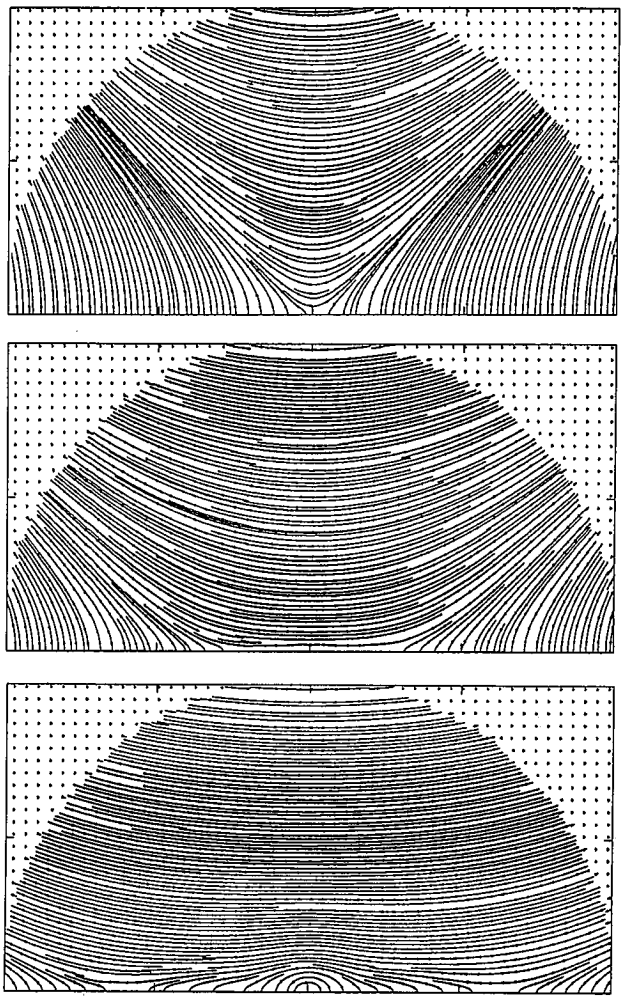

Fig. 8. Line segments drawn parallel to the magnetic field lines. The beginning and end of the lines are selected internally by the plot package, and consequently, the fact that the lines end suddenly does not imply the sudden appearance or disappearance of a magnetic field line. The solution in this and the following figure is symmetric about the lower axis in each panel and is shown at times of 5.4 τ_a, 8.8 τ_a, and 9.9 τ_a from top to bottom.

incompressible nonlinear MHD equations and for two distinctly different sets of outer boundary conditions. The qualitatively similar results obtained with the compressible and incompressible simulations demonstrates that the thermodynamics does not play a significant role in the evolution of x-points. When the boundary consists of a solid, conducting wall, the perturbed x-point relaxes back to the unstressed state on a time scale proportional to the resistivity. The decay time scale computed here for small perturbations agrees with earlier analytic linear studies and is somewhat faster than the time scale for reconnection in the resistive tearing instability. When the boundary is open, so conditions at the boundary can adjust to the evolution near the x-point, the perturbation grows in amplitude on an Alfvén time scale. The initial x-point evolves into a current sheet separating y-points at the ends of the sheet. The y-points propagate away from each other into regions of increasing magnetic field strength.

Acknowledgments. This work was supported by National Science Foundation Grant No. ATM-90-15705 and at the Institute for Fusion Studies by U.S. Department of Energy Contract No. DE-FG05-80ET-53088.

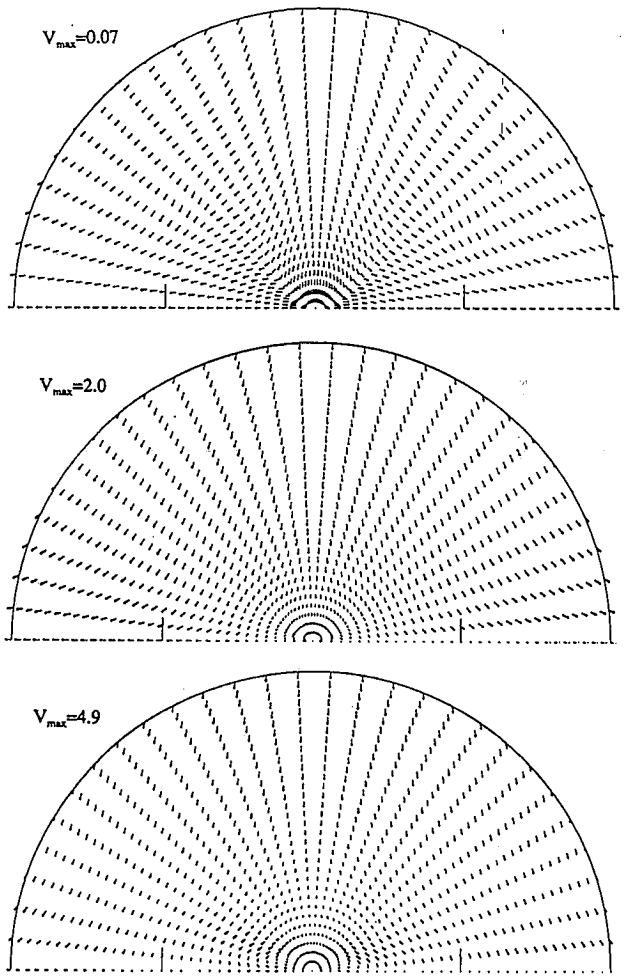

Fig. 9. Velocity vectors for the solution shown in Figure 8. The length of the velocity vectors at each time is scaled to the maximum speed throughout the grid, which is indicated by the given value of V_{max}.

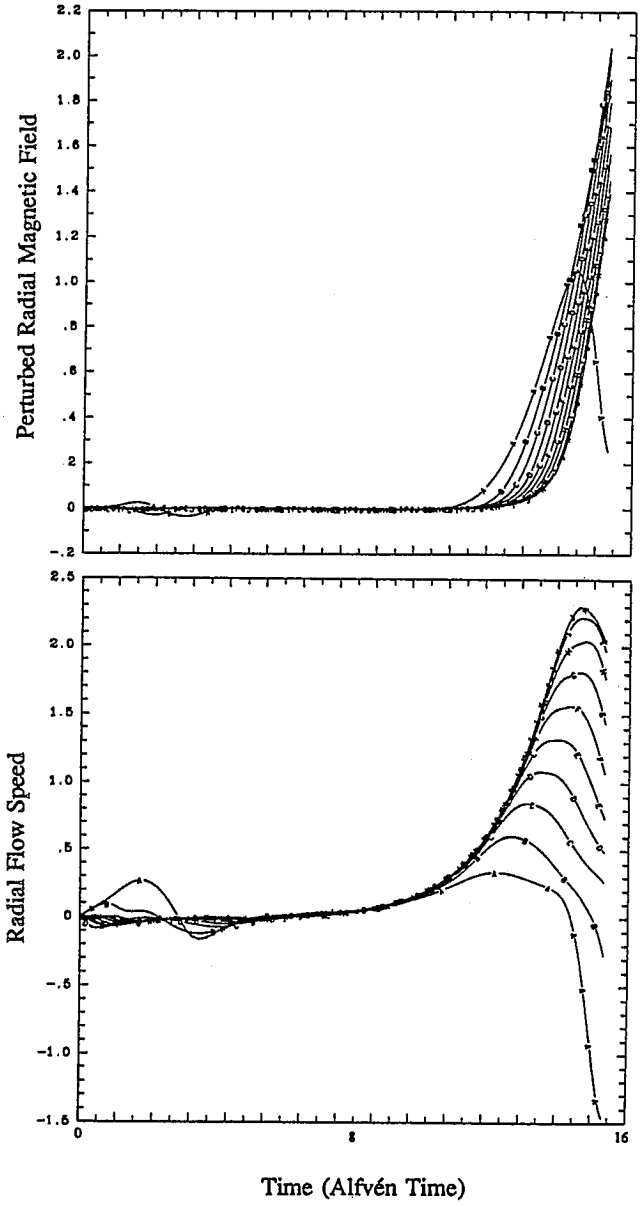

Fig. 10. The time variation of the radial components of the magnetic field and velocity at $\theta = 10°$ and at several radial locations spaced evenly between $r = 0.2$ and $r = 2.0$.

REFERENCES

Akasofu, S. -I., and S. Chapman, A neutral line discharge theory of the aurora polaris, *Phil. Trans. A, 253*, 44-49, 1961.

Chapman, S., and P. C. Kendall, Liquid instability and energy transformation near a magnetic neutral line: a soluble non-linear hydromagnetic problem, *Proc. Roy. Soc., A271*, 435-448, 1963.

Craig, I. J. D., and A. N. McClymont, Dynamic magnetic recon nection at an x-type neutral point, *Astrophys. J., 371*, L41-L44, 1991.

Craig, I. J. D., and P. G. Watson, Fast dynamic reconnection at x-type neutral points, *Astrophys. J., 393*, 385-395, 1992.

Dungey, J. W., Conditions for the occurrence of electrical discharges in astrophysical systems, *Phil. Mag., 44*, 725-738, 1953.

Furth, H. P., J. Killeen, and M. N. Rosenbluth, Finite-resistivity instabilities of a sheet pinch, *Phys. Fluids, 6*, 459-484, 1963.

Giovanelli, R. G., Magnetic and electric phenomena in the Sun's atmosphere associated with sunspots, *Mon. Not. R. Astro. Soc., 107*, 338-355, 1947.

Hassam, A. B., Reconnection of stressed magnetic fields, *Astrophys. J., 399*, 159-163, 1992.

Lapidus, A., A detached shock calculation by second-order finite differences, *J. Comput. Phys., 2*, 154-177, 1967.

Ofman, L., Resistive magnetohydrodynamic studies of tearing mode instability with equilibrium shear flow and magnetic reconnection, *IFSR 552*, Univ. of Texas, PhD. Thesis, 1992.

Parker, E. N., Kinematical hydrodynamic theory and its application to the low solar photosphere, *Astrophys. J., 138*, 552-575, 1963.

Rubin, E. L., and S. Z. Burstein, Difference methods for the inviscid and viscous equations of a compressible gas, *J. Comput. Phys., 3*, 178-196, 1967.

Steinolfson, R. S., and G. van Hoven, Nonlinear evolution of the resistive tearing mode, *Phys. Fluids, 27*, 1207-1214, 1984.

Sweet, P. A., The neutral point theory of solar flares, in *Electro magnetic Phenomenon in Cosmical Physics*, edited by B. Lehnert, pp. 123-140, Cambridge University Press, New York, 1958.

Syrovatskii, S. I., Dynamic dissipation of a magnetic field and particle dissipation, *Soviet Astron., 10*, 270-280, 1966.

L. Ofman and P.J. Morrison, Department of Physics and Institute for Fusion Studies, The University of Texas at Austin, austin, TX 78712.

R. S. Steinolfson, Department of Space Science, Southwest Research Institute, PO Drawer 28510, San Antonio, TX 78228-0510.